博士論文

Molecular mobility inside dendritic spines of cultured hippocampal neurons investigated by two photon raster image correlation spectroscopy

（2 光子 RICS 法による海馬神経細胞スパイン内分子動態解析）

小橋　一喜

Table of contents

1. Abstract 2

2. Introduction 4

3. Materials and Methods 10

4. Results 18

5. Discussion 28

6. References 35

7. Acknowledgements 46

8. Figure legends 47

9. Figures 54

Abstract

The amount, nano-scale localization, and dynamic behavior of molecular complexes inside dendritic spines may influence synaptic functions both in a resting state and under synaptic plasticity. Here, I measured dynamics of biologically inert probes (EGFP and tandem EGFP pentamer (EGFP5)) with different molecular sizes inside dendritic spines of cultured neurons using two-photon raster image correlation spectroscopy (RICS). From the RICS correlation function, the fraction sizes of fast and slow components and their diffusion coefficients can be estimated. RICS could reliably measure molecular mobility in larger cellular compartments, such as soma. The diffusion coefficient of fast EGFP5 component inside spines was independent of spine volume. And it was comparable with that inside soma and dendritic shafts. These results suggest that RICS can be used to estimate molecular mobility even inside small cellular compartments, such as dendritic spines. If spine contains any structural components that hinder mobility of large molecules, this structural characteristics may change the relative proportion of fast and slow components. Indeed, slow mobile fraction was found to be a major component in spines but a minor component in dendritic shafts. The slow mobile fraction was larger in the case of EGFP5 than EGFP. The structural barrier within spines may be related to the actin cytoskeleton, as treatment with an actin-depolymerizing reagent decreased the size of slow mobile fraction. In summary, RICS is useful in reporting molecular dynamics within small

cellular compartments and the mobility of macromolecules with their sizes of >150 kDa may be restricted within spines by the actin-dependent mechanism.

Introduction

Neurons communicate with each other through a specialized structure called synapse and modulation of synaptic connectivity is important in brain functions. In the case of mammalian neocortex and hippocampus, excitatory synapses are formed onto dendritic spines of the pyramidal neuron. Spines are tiny protrusions, with a roughly spherical head (0.5-1.5 μm in diameter) connected by a narrow neck (<0.5 μm in diameter) to dendritic shafts (Yuste, 2010). The spine necks serve as diffusion barrier (Bloodgood and Sabatini, 2005, Tønnesen et al, 2014), and spines function as a biochemical compartment (Newpher and Ehlers, 2009). Dendritic spines contain post synaptic densities, the actin cytoskeleton and cellular organelles (Sheng and Hoogenraad, 2007). Spines contain hundreds of functional molecules (Sala and Segal, 2014) and their localization and dynamics provide a basis for signal transduction both in a resting state and under synaptic plasticity. Therefore, it is important to precisely measure the amount, nano-scale localization, and dynamic behavior of structural components within spines. Due to the small size of spines and limitations of available techniques, the quantitative properties of postsynaptic molecules and cytoskeletal polymers are just beginning to be understood (MacGillavry and Hoogenraad, 2015). The spatial resolution of conventional fluorescent microscopy (~250 nm in lateral and ~1 μm in axial) is comparable to the size of spines. Therefore its application to the quantitative analysis of intra-spine components has been limited.

Recently, superresolution microscopy and electron microscopy (EM) provided information about distribution of synaptic molecules and structures of intra-spine filamentous actin (F-actin) (Dani et al., 2010, Rácz and Weinberg, 2013). Since the temporal-resolution of superresolution microscopy is still limited, present superresolution techniques are not appropriate for the measurements of molecular dynamics inside spines.

In order to be able to faithfully monitor the dynamics of intra-spine components, development of novel optical techniques is needed. Intracellular translational mobility of fluorescent probes can be measured by quantitative optical techniques such as fluorescence recovery after photobleaching (FRAP), fluorescence correlation spectroscopy (FCS) and their related methods (Kim et al., 2010, Lin et al., 2013). Several of these methods have been applied to measure the molecular mobility inside dendritic spines. In FRAP measurements, fluorescent molecules in a small region of the cell are irreversibly photobleached and subsequent movement of surrounding non-bleached fluorescent molecules into the photobleached area is recorded. From the recovery kinetics, molecular mobility can be estimated (Lippincot-Schwartz et al., 2001). FRAP is suitable to measure the molecular replacements that takes place in a time range of seconds to hours. The turnover of synaptic proteins inside dendritic spines have been investigated by FRAP (Star et al., 2002, Kuriu et al., 2006, Sharma et al., 2006). Recently, FRAP measurements of fluorescent proteins and Alexa dyes, have been reported in combination with precise

determination of spine structures (Bloodgood and Sabatini, 2005, Tønnesen et al., 2014). In these experiments, the bleached volume was comparable to the size of entire spines. Therefore, the diffusional coupling between spines and dendritic shafts was a major determinant of FRAP recovery kinetics. In combination with superresolution microscopy, these reports revealed that width of spine neck was the major parameter for this diffusional coupling (Tønnesen et al., 2014).

To directly investigate intra-spine molecular mobility, techniques other than FRAP are needed. FCS and image correlation techniques are promising candidates. In FCS experiments, the fluctuation of fluorescence intensity from the detection volume fixed at a specific intracellular position is recorded as a function of time and then transformed to an autocorrelation curve. By fitting the curve to an appropriate physical model, information about diffusion coefficients, local concentration, states of aggregation and molecular interactions can be estimated (Kinjo et al., 2011, Bacia et al., 2014). Since FCS detection volume is small, I assumed that it is possible to measure intra-spine molecular mobility using FCS. Recently, a two-photon FCS measurement of EGFP-actin mobility inside spines has been reported (Chen et al., 2015). As an extension of FCS, raster image correlation spectroscopy (RICS) has been developed for measurements of molecular mobility inside cells (Digman et al., 2005). In RICS measurements, spatial correlation was calculated from a series of raster scanned images. By calculating the spatial correlation

between pixels of raster scanned images, information about molecular mobility can be extracted from the correlated signals both in spatial and temporal domains using an appropriate physical model, as in the case of FCS.

Comparing FCS and RICS, RICS has potential advantage for measurements inside spines. FCS needs stable localization of the focal volume inside spine heads during the recording. Because measurement time should be extended for slowly moving populations (Kim et al., 2007), intra-spine FCS measurement of slowly-moving molecules is difficult. On the other hand, in RICS experiments, ROI can be selected after imaging and evaluating structural changes of spine. Because spines are dynamic structure, this feature of RICS can be beneficial for intra-spine measurements.

Molecular mobility in cellular compartments deviates from what is observed in dilute solutions. For example, translational diffusion coefficient of EGFP in cytoplasm was 3-4 times slower than that in solution (Swaminathan et al., 1997, Pack et al., 2006). Regulation of molecular mobility is thought to be important for intracellular signaling from several reasons (Verkman, 2002). First, suppression of molecular mobility is needed for compartmentalized biochemical reactions. Second, suppression of molecular mobility reduces an encounter rate of signaling molecules. Because the composition, geometry, and solvent properties of the intracellular environment determine the characteristics of molecular diffusion (Luby-Phelps, 2000, Lin et al., 2013), understanding the cytoplasmic

structure which hinder molecular mobility is also important. Cytoplasm is crowded with small solutes, soluble macromolecules, cytoskeletal filaments and membranes (Medalia et al, 2002). In addition to viscosity of cytoplasm, binding and collision to intracellular components reduce apparent diffusion coefficient (Baum et al., 2014, Di Rienzo et al., 2014). The difference of molecular mobility among probes with variable sizes has been used for investigating cytoplasmic structures (Luby-Phelps et al., 1986, Popov and Poo, 1992, Seksek et al., 1997). Combining a line illumination with parallelized FCS, Baum et al. (2014) retrieved the intracellular structure of human U2OS cells from the scale-dependent mobility of EGFP monomers (hydrodynamic radius (r_H) ≈ 2.8 nm), trimers (EGFP3, r_H ≈ 5.5 nm) and pentamers (EGFP5, r_H ≈ 7.9 nm). The authors found that the anomalous diffusion behavior changed from EGFP to EGFP5, revealing a protein size dependence of the accessible cellular space. Disassembly of F-actin by cytochalasin-D treatment has a moderate effect on EGFP3 mobility in the cytoplasm. This suggests that other cytoplasmic components, such as cellular organelles, are main obstacles that restrict cytoplasmic mobility (Novak et al., 2009). In another series of study, translocation through the cytoplasm of the axon initial segment (AIS) of cultured neurons was measured by FRAP (Popov et al., 1992, Song et al., 2009). After 5 days *in vitro* (DIV), a diffusion barrier was emerged at AIS and it suppressed movement of 70 kDa dextran (r_H ≈ 6.4 nm), but did not affect movement of 10 kDa dextran (r_H ≈ 3.9 nm). This AIS diffusion barrier

was eliminated by F-actin disrupting reagents. These results indicate that the AIS diffusion barrier was F-actin dependent network and its mesh size was estimated to be less than 13 nm. Dendritic spines also contain dense F-actin network (Hotulainen and Hoogenraad, 2010). Therefore, it is reasonable to postulate that molecular mobility inside dendritic spines is hindered through steric interaction with intra-spine components.

In this study, I aimed at identifying intra-spine nanostructures that affect mobility of macromolecules and conducted two photon RICS measurements of fluorescent proteins within cultured hippocampal neurons. I first confirmed that two photon RICS can reliably measure molecular mobility in larger cellular compartments, such as soma of neurons. Next I performed RICS measurements of EGFP or EGFP5 inside dendritic spines and dendritic shafts. Fitting of the spatial correlation from RICS measurements revealed that the fraction of molecules with slower mobility was estimated to be a major fraction in dendritic spines but a minor fraction in dendritic shafts. This slow mobile fraction was larger in neurons expressing EGFP5 than in neurons expressing EGFP. Depolymerization of F-actin with latrunculin A decreased the slow mobile fraction. These results imply that the intra-spine actin cytoskeleton was one of the factors contributing to modulation of molecular mobility within spines.

Materials and methods

Molecular constructs

Tandem EGFP pentamer (EGFP5) plasmid was provided by Dr. Masataka Kinjo (Hokkaido University, JAPAN) (Pack et al., 2006). The DNA fragments containing coding regions of EGFP, EGFP5 and mRFP were inserted into the expression plasmids containing β-actin promoter sequences (Ebihara et al., 2003).

Hippocampal neuronal cultures, gene expression and drug treatment

Cultures of hippocampal neurons from 17-day-old embryonic mice were prepared as described previously (Okabe et al., 1999). Transfection of hippocampal neurons was performed by a Ca^{2+}-phosphate transfection method at 7-8 DIV (Jiang and Chen, 2006). All experiments were performed at 18-23 DIV. Hippocampal neurons were measured in imaging solution (140 mM NaCl, 5 mM KCl, 2 mM $CaCl_2$, 2 mM $MgSO_4$, 5 mM HEPES and 20 mM glucose (pH 7.4)) at 25°C. Latrunculin A (Molecular Probes, Eugene, OR) solved in dimethylsulfoxide (DMSO) was used at final concentration of 2 μM.

Immunocytochemistry

Hippocampal neurons were fixed in 2% paraformaldehyde in phosphate buffered saline for 25 min, permeabilized with 0.2% Triton X-100 for 5 min, blocked with 5% normal goat

serum for 30 min and reacted with mouse monoclonal antibody to GFP (Molecular Probes, Eugene, OR, USA). The primary antibody was visualized by secondary antibody staining with goat anti-mouse IgG conjugated to Cy3 (Molecular Probes, Eugene, OR, USA).

Confocal imaging and FRAP experiments

Imaging of fluorescent proteins and anti-GFP staining and FRAP experiments were performed by a Fluoview twin-scanner confocal laser-scanning microscope with ×60 0.9 NA water immersion objective lens (Olympus, Tokyo, JAPAN). Images were collected in a lateral spatial resolution of 103 nm per pixel. For imaging, a confocal aperture was set at a diameter of 170 μm (the size of 1 Airly disk). Multiple optical sections (5-9 sections and z-spacing of 0.75 μm) were collected, and these images were recombined using a maximum-brightness projection for further analysis. Image analysis and quantification were performed by using ImageJ (NIH, Bethesda, MD, USA). Fluorescence intensities of dendritic spines and dendritic shafts were measured as sums of pixel intensities in 15 × 15 pixel (~1.5 × 1.5 μm^2) rectangular regions manually selected regions after subtraction of background intensities. For FRAP experiments, a confocal aperture was set at a diameter of 450 μm. Images were taken at 2 Hz for 75 frames and photo bleaching was achieved by the second laser line. Fluorescence intensities of dendritic spines were measured as sums of pixel intensities in 15 × 15 pixel (~1.5 × 1.5 μm^2) rectangular regions manually centered

on individual spines after subtraction of background intensities. All fluorescent values were subtracted by the first post-bleach value and then were normalized by the average pre-bleached values. The first post-bleach measurement was set to t = 0 sec. Fluorescence recovery curves were fitted with single-exponential function for EGFP and with dual exponential function for EGFP5.

Two-photon laser scanning microscopy

RICS and FCS measurements were performed by a custom build two-photon laser scanning microscope. The microscope was constructed with a BX50WI upright microscope (Olympus, Tokyo, Japan) and a pulsed Ti::sapphire laser (Tsunami, Spectra Physics, Tokyo, Japan) tuned to 880 nm. The laser power were attenuated by a metallic neutral density filter. 9 mW of power in the back aperture of objective lens was used for FCS and RICS experiments. The laser was guided into the microscope by x, y galvano scanner mirrors (6210H, GSI, Bedford, MA, USA). The beam transmitted through a dichroic mirror (FF735-Di01, Semrock, Rochester, NY, USA) towards a water immersion objective (LUMFI, 1.0 NA, Olympus, Tokyo, Japan). Z-position of the objective was controlled by a piezoelectric objective positioner (P-725.1CL, PI, Tokyo, Japan). The fluorescence emission was collected by the same objective and reflected by the dichroic mirror. The fluorescence transmitted through a short path filter (et750sp-2p, Chroma, Rockingham,

VT, USA) was detected by a photon counting photomultiplier tube (PMT) (H7421-40, Hamamatsu photonics, Hamamatsu, Japan) as a non-descanned collection. To control microscope's devises and acquire fluorescent signals, a data acquisition board (PCIe-6363, National Instruments) controlled by a custom written software (Visual studio, Microsoft, Seattle, WA, USA) was used. For FCS measurements, output signal from PMT was acquired by a hardware correlator (ALV-7004, ALV, Langen, Germany).

FCS measurements and analysis

FCS signal was measured for 10 sec three times in a series or 30 sec and fluorescence autocorrelation function (G(τ)) was gained:

$$G(\tau) = \frac{<F(t)F(t+\tau)>}{<F(t)>^2} - 1 \qquad (1)$$

where F(t) is the fluorescence intensity observed from the two-photon excitation volume at the time t and τ is the correlation time. Brackets denote ensemble averages (Schwille et al., 1999, Pack et al., 2006). Data analysis was conducted according to the previous papers (Pack et al., 2006, Kim et al., 2007). To obtain the diffusion time (τ_i), the autocorrelation function was fitted by the following multi-component model:

$$G(\tau) = 1 + \frac{1}{N}\sum_i f_i\left(1 + \frac{\tau}{\tau_i}\right)^{-1}\left(1 + \frac{\tau}{(z_0/w_0)^2\tau_i}\right)^{-1/2} \qquad (2)$$

Where f_i is the fraction of component i. N is the number of fluorescent molecules in the detection volume defined by the beam waist w_0 and the axial radius z_0. The detection

volume made by w_0 and z_0 was approximated as a cylinder. A one-component model was used for solution experiments and a two-component model was used for intracellular experiments. Diffusion time is related to the translational diffusion constant D_i by

$$\tau_i = \frac{{w_0}^2}{8D_i} \qquad (3)$$

The D of EGFP (or EGFP5) was calculated from the reported value of D of Rhodamine 6G (D_{Rh6G} = 280 $\mu m^2/s$), and the measured values of the diffusion times of Rh6G (τ_{Rh6G}) and EGFP (τ_{EGFP}), as follows:

$$\frac{D_{EGFP}}{D_{Rh6G}} = \frac{\tau_{Rh6G}}{\tau_{EGFP}} \qquad (4)$$

RICS measurements and analysis

RICS is a type of the image correlation spectroscopy (Digman et al., 2005). Spatial autocorrelation function of RICS is calculated from a stack of images obtained by laser scanning fluorescence microscopy. The RICS correlation function is calculated as follows:

$$G(\xi, \psi) = \frac{<F(x,y)F(x+\xi,y+\psi)>}{<F(x,y)>^2} - 1 \qquad (5)$$

where F(x,y) is the fluorescence intensity at pixel located at x, y of the image and ξ and ψ are spatial increments in the x and y directions of the image. This correlation function contains information about the probability that a molecule detected at position (x,y) is also detected at position ($x+\xi$,$y+\psi$) after the delay of $\tau_p\xi+\tau_l\psi$, where τ_p is pixel duration and τ_l is line interval respectively. This probability depends on scanning properties (pixel size (δ),

pixel duration and line interval) and movement of the molecule. The movement of the molecule is independent from the scanning properties. Therefore, the RICS correlation function is written as the product of the molecular movement information ($D(\xi,\psi)$) and the laser scanning information ($S(\xi,\psi)$).

$$G(\xi,\psi) = \frac{1}{N}\sum_i f_i D_i(\xi,\psi) S_i(\xi,\psi) \quad (6)$$

$$D_i(\xi,\psi) = \left(1 + \frac{\tau_p\xi + \tau_l\psi}{\tau_i}\right)^{-1}\left(1 + \frac{\tau_p\xi + \tau_l\psi}{({}^{z_0}/_{w_0})^2\tau_i}\right)^{-1/2} \quad (7)$$

$$S_i(\xi,\psi) = \exp\left(\frac{({}^{\delta}/_{w_0})^2(\xi^2+\psi^2)}{1+{}^{\tau_p\xi+\tau_l\psi}/_{\tau_i}}\right) \quad (8)$$

Figure 1 shows that how different molecular diffusion mobility appears in the RICS correlation function under the imaging condition used in this study. The shapes of the RICS correlation functions are changed depending on the diffusion coefficients (Fig. 1A). The RICS correlation function contains two different time scale information; microsecond time scale for horizontal scanning axis (x-axis) and millisecond time scale for vertical scanning axis (y-axis). X-axis correlation is sensitive to faster moving molecules in a range of 1-10 $\mu m^2/s$. This is derived from the relative speed of molecular diffusion and x-axis scanning velocity. X-axis correlation becomes smaller as the molecular diffusion becomes faster (Fig. 1B). For slowly moving molecules, x-axis profile of the RICS correlation functions ($G(\xi,0)$) almost stay constant and similar to PSF (D = 0.01-1 $\mu m^2/s$ in Fig. 1B; Brown et al., 2008). On the other hand, y-axis profile of the RICS correlation functions ($G(0,\psi)$) is more sensitive to slowly moving molecules with their D of 0.01 $\mu m^2/s$ to 10 $\mu m^2/s$ (Fig.

1C).

For RICS experiments, 30 frames consisting 256 × 256 pixels were collected. The pixel size is 17 nm. The pixel dwell time is 40 μs and line intervals is 15.36 ms respectively. For measurements of dendritic spines and dendritic shafts, 64 × 64 pixel (~1.1 × 1.1 μm^2) rectangular regions manually selected from the image stacks. For calculation of the RICS correlation function and curve fitting were done with ImageJ plugin developed and distributed by Dr. Jay Unruh (Stowers Institute for Medical Research, USA). To remove the immobile features, stack images were subtracted by five frames rolling average and then added by the average image intensity (Digman et al., 2005). After this image processing, the RICS correlation function was calculated. When images were collected without samples, x-axis of the RICS correlation functions contain positive correlation in the first two frames. Therefore, for curve fitting, the first two pixels of the RICS correlation were removed from the fitting process (Brown et al., 2008, Rossow et al., 2010). The detection volume information using the curve fitting was estimated from FCS measurements of Rhodamine-6G solution. For curve fitting of the RICS correlation function from dendritic spine and shaft measurements, center 20 × 20 pixels of the correlation functions are used for fitting due to the size of spines and shafts.

Quantification of spine neck length and cross section area

Fluorescence intensity was measured along the ~500 nm width line passing through spine head, neck and shaft. Then line profile was fitted by two Gaussian functions. Positions which show one-half of each peak amplitude were defined as the edges of the spine head and shaft (Matsuzaki et al., 2001). The spine neck length was defined as the distance between the edges of the spine head and shaft, and the spine neck volume was defined as sums of pixel intensities between the edges of the spine head and shaft after subtraction of background intensities. When the spine neck length was negative value, that spine was excluded from the further analysis. The spine neck cross section area was estimated by the spine neck volume divided by the spine neck length.

Statistical analysis

Data are presented as means ± standard error. Statistical significance was determined by performing paired t-test for comparing two samples. All statistical analysis and curve fitting were performed using Origin (Light Stone, Tokyo, JAPAN).

Results

EGFP5 accumulated inside dendritic spines not due to non-selective absorption to the cytoplasmic structures

To examine the existence of cytoplasmic architecture that hinders molecular mobility inside dendritic spines, different sizes of biologically inert probes (mRFP and EGFP5) were transfected to hippocampal neurons in culture (Fig. 2A). A hydrodynamic radius of mRFP is a similar to that of EGFP (Baum et al., 2014). So in this study mRFP behavior in the cytoplasm was considered to be the same as that of EGFP. Less fluorescence signal from dendritic spines compared with dendritic shafts in neurons expressing mRFP is consistent with the distribution of inert fluorescent probes in previous reports. However, EGFP5, whose molecular weight 5-fold higher than mRFP, showed stronger fluorescence signal within dendritic spines. If EGFP fluorescence intensity changes in different intracellular compartments, higher fluorescence signals from spines may not reflect the actual density of molecules. To estimate molecular density of EGFP5 and EGFP in dendritic spines and shafts, EGFP or EGFP5 expressing neurons were stained with anti-GFP antibody and Cy3-conjugated secondary antibody (Fig. 2E). The overall staining pattern with anti-GFP antibody was similar to EGFP or EGFP5 fluorescence images. The ratio of EGFP-derived fluorescence against Cy3 fluorescence was similar between spines and shafts in neurons expressing either EGFP or EGFP5 (Fig. 2F). This result suggests that

EGFP fluorescence reliably reports the local concentration of EGFP protein. Therefore, the stronger EGFP5 signal within spines indicates accumulation of inert fluorescent probes with a higher molecular weight within a small cytoplasmic space separated from dendritic shafts. Application of latrunculin A, F-actin depolymerizing agent, decreased the EGFP5 accumulation inside dendritic spines (Fig. 2C) and also decreased the spine volume (Fig. 2D). Since the fluorescence intensity ratio between mRFP and EGFP5 was constant regardless of spine size, EGFP5 was accumulated even in the small spines (Fig. 2B). To determine whether EGFP5 accumulation is caused by non-selective absorption to the cytoplasmic structures, FRAP measurements were conducted on dendritic spines of EGFP-expressing neurons (Fig. 3A) and EGFP5-expressing neurons (Fig. 3B). The recovery of EGFP5 reached a steady state within 10 sec and the mobile fraction of EGFP5 was comparable to that of EGFP. The data are not consistent with the idea that non-selective absorption of EGFP5 to the cytoplasmic structures is the main cause of EGFP5 accumulation. EGFP recovery curve was fitted with an exponential function with a single time constant 0.33 ± 0.02 sec. This value is consistent with previously reported values (Bloodgood and Sabatini, 2005, Tønnesen et al., 2014). On the other hand, therefore the recovery curve of EGFP5 could not fit well with a single component model, a two-component model was used (Fig. 3C). From the difference of reported diffusion coefficients in solution and inside the cytoplasm of cell lines (Pack et al., 2006), the

estimated time constant of EGFP5 is 0.8 sec. The time constant of fast fraction was in a similar range with the estimation, but this fast fraction was not a major component. On the other hand, the major component of the fluorescence recovery showed much slower time constant of 4.4 sec, which was more than 5-times larger than the estimated value. This reduction in mobility was partially recovered by latrunculin A treatment (Fig. 3B, C). These results may be consistent with the idea that EGFP5 mobility is hindered by intra-spine F-actin polymers that selectively affect molecules with higher molecular weights. However, the effect of spine neck for the EGFP5 accumulation should also be take into account, as the molecular exchange rate between spines and shafts should be dependent highly on the diameters, lengths, and curvature of spine necks. In order to exclude the contribution of spine neck geometry, direct readout of molecular diffusivity inside the spine cytoplasm is needed.

RICS measurements of neurons expressing EGFP or EGFP5

FCS is a sensitive method for measuring diffusion constants of fluorescent molecules inside small focal volumes. To investigate intra-spine molecular mobility directly, I tried FCS measurements inside dendritic spines of EGFP5 expressing neurons. However, excessive photobleaching occurred and reliable FCS measurements were difficult, if not impossible (data not shown). Therefore I switched to RICS as an alternative method

because RICS is an optical technique based on focal volume scanning and expected to be less prone to induce photobleaching (Abdisalaam et al., 2013).

On RICS measurements, the imaging conditions including pixel size, pixel duration and line interval should be set appropriately to capture the movement of target fluorescent molecules. Using Dextran70kDa-RhadamineB dissolved in the imaging solution, of which diffusion coefficient is similar to that of intracellular EGFP, I first optimized the RICS procedure by comparing results from FCS and RICS (Fig. 4A, B; see Materials and Methods). Next, to confirm whether the procedure optimized for measurements of fluorescently labeled dextran solution is applicable to the measurements of intracellular EGFP and EGFP5 mobility, molecular mobility inside soma of neurons expressing EGFP (Fig. 4C-E) or EGFP5 (Fig. 4F-H) were measured by FCS and RICS. Correlation functions obtained from measurements of EGFP and EGFP5 were fitted by a two-component model. The first component corresponded to the fast moving component and was the major fraction (> 85%). Diffusion coefficients of the first components (D_1) obtained from two independent methods were comparable. Therefore, I concluded that the EGFP and EGFP5 mobility at least inside large neuronal compartments could be measured by RICS.

EGFP5 mobility differs between inside dendritic spines and shafts

RICS measurements were done inside dendritic spines and shafts of EGFP5 expressing

neurons (Fig. 5). After collecting image series of 256 × 256 pixels (~4.4 × 4.4 μm^2), I selected 64 × 64 pixel (~1.1 × 1.1 μm^2) rectangular regions containing spine heads or shaft regions and calculated RICS correlation functions (Fig. 5A). Interestingly, the RICS correlation functions from spine region were completely different from those from shaft region. The y-axis correlation was prominent only for spine regions. To compare RICS correlation functions from spine regions with those from shaft regions, the data were fitted with a two-component model (Fig. 5B-D). Diffusion coefficient of the first (fast) component (D_1) from spine regions was slightly larger than that from shaft regions ($p=0.07$). This slight difference might be occurred due to focal volume confinement effect by small spine volume (Gennerich and Schild, 2000, Foquet et al., 2004). Even so, these values were comparable with diffusion coefficients of the first component from cytosol of soma (Fig. 4H). Diffusion coefficients of the second (slow) component (D_2) from spine regions were smaller than from shaft regions (Fig. 5C). Contribution of the first component (f_1) of spine region was smaller than that of shaft regions (Fig. 5D). This result was reproducible even when fitting of spine correlation function was done with fixed diffusion coefficients of shaft measurements, eliminating the possibility that our estimation of diffusion coefficients within spines was biased and caused underestimation of fractions. Relationship among fitting parameters from spine measurements were analyzed (Fig. 5E-G). There was a tendency that smaller D_1 values are associated with larger f_1 values. This

relationship may be related to the difficulty in appropriate curve fitting when RICS correlation functions showed low signal-to-noise ratio.

Detection of slow moving EGFP5 inside dendritic spines is independent from spine volume, spine neck length and cross section area variation

RICS reported the existence of a large fraction of slow moving EGFP5 only inside dendritic spines. To check the possibility that this result comes from the spine morphology, spine structural parameters and results from RICS measurements were compared. First, relationship between spine volume and fitting results from RICS correlation functions was analyzed. Because spine fluorescence intensity of EGFP5 and mRFP showed a linear relationship (Fig. 2B), spine fluorescence intensity of EGFP5 was used as index of spine volume, instead of expressing mRFP as an independent volume marker. In order to normalize spine fluorescence intensity from images of independent experiments, spine fluorescence intensities were normalized by an average value of all spines in the same dendrites (10-18 spines in each image). Spine volume was not correlated with D_1, D_2 and f_1 (Fig. 6A-C). The slow mobility component was detected regardless of spine volumes. This is consistent with the result that the rate of spine EGFP5 accumulation was uniform regardless of spine volume (Fig. 2B). In addition, relationship between spine volume fluctuation and the fitting results was analyzed. The same spine was measured twice for 10

min intervals. Change of spine volume was not correlated with change of D_1, D_2 and f_1 (Fig. 6D-F). In summary, EGFP5 mobility measured by RICS was not influenced by spine volume difference.

Next, relationship between spine neck morphology and results from RICS measurements was analyzed. Spine neck length (Fig. 7A-C) and spine neck cross section area (Fig. 7D-F) were not correlated with D_1, D_2 and f_1. Relationship between fluctuations of spine neck cross section area and fluctuations of the fitting parameters was also analyzed. This was based on the 10 min intervals imaging data used for spine volume fluctuation analysis (Fig. 6D-F). Change of spine neck cross section area was not correlated with changes of D_1, D_2 and f_1 (Fig. 7G-I). These results indicated that molecular mobility measured by RICS was not changed by spine neck morphology and supported the notion that RICS can measure molecular mobility inside the spine in contrast to FRAP. These analyses indicated that spine morphological features including spine volume, spine neck length and cross section area were not main cause of detecting EGFP5 slow mobility inside spines by RICS.

Intra-spine F-actin cytoskeleton modulate EGFP5 mobility

F-actin is the main cytoskeletal architecture of dendritic spines. And application of latrunculin A decreased the EGFP5 accumulation inside dendritic spines (Fig. 2C).

Therefore, intra-spine F-actin may hinder EGFP5 mobility through steric interaction. To examine this possibility, RICS measurements were conducted before and after latrunculin A treatment (Fig. 8A-D). EGFP5 expressing neurons were imaged twice before pharmacological treatment and three times after the treatment with intervals of 10 minutes. The first imaging time point of post pharmacological treatment was 20 minutes after application. The RICS correlation functions from spines and shafts were not identical and there existed a considerable difference in the fraction contribution of the first component (f_1) (Fig. 5D). From this relationship, I considered f_1 as reference index of molecular movement suppression. For spine measurements, D_1 was decreased by latrunculin A treatment (pre: $D_1 = 4.33 \pm 0.39$ $\mu m^2/s$, post: $D_1 = 2.53 \pm 0.33$ $\mu m^2/s$), not by DMSO (pre: $D_1 = 4.33 \pm 0.46$ $\mu m^2/s$, post: $D_1 = 4.13 \pm 0.39$ $\mu m^2/s$). Because D_1 and f_1 were weakly correlated (Fig. 5F), change of D_1 can potentially affect the f_1 value. To test this possibility, I repeated the curve fitting and estimation of f_1 using the same data set but with D_1 and D_2 set at the values estimated from shaft measurements (Fig. 8E, F). The results from shaft measurements were not changed by DMSO and laturunculin A treatments (pre DMSO: $D_1 = 3.37 \pm 0.16$ $\mu m^2/s$, $D_2 = 0.06 \pm 0.01$ $\mu m^2/s$, $f_1 = 83.6 \pm 1.8\%$, post DMSO: $D_1 = 3.17 \pm 0.15$ $\mu m^2/s$, $D_2 = 0.07 \pm 0.01$ $\mu m^2/s$, $f_1 = 80.9 \pm 2.3\%$, pre Lat: $D_1 = 3.32 \pm 0.26$ $\mu m^2/s$, $D_2 = 0.04 \pm 0.02$ $\mu m^2/s$, $f_1 = 90.2 \pm 1.5\%$, post Lat: $D_1 = 3.56 \pm 0.28$ $\mu m^2/s$, $D_2 = 0.05 \pm 0.01$ $\mu m^2/s$, $f_1 = 88.4 \pm 1.2\%$, for all pairs $p>0.05$). On the other hand, latrunculin A treatment

increased f_1 value of spine regions. This change was reproducible when the curve fitting was conducted with free D_1 and D_2 values (pre DMSO: $f_1 = 44.9 \pm 1.4\%$, post DMSO: $f_1 = 45.2 \pm 1.3\%$, pre Lat: $f_1 = 46.6 \pm 1.9\%$, post Lat: $f_1 = 64.1 \pm 1.7\%$). These results indicated that EGFP5 movement is hindered by intra-spine F-actin. This also supports the idea that slow movement of EGFP5 inside dendritic spines is due to physical barrier present within spines, not simply due to small spine volume.

Mobility suppression by intra-spine F-actin cytoskeleton depends on molecular size

If molecular mobility is suppressed by F-actin inside dendritic spine, it would be predicted that this effect is less for smaller molecule. To test this possibility, I next conducted RICS measurements of EGFP inside dendritic spines and shafts (Fig. 9A, B). As expected, the y-axis correlation of spine region was less prominent in comparison with EGFP5 measurements. Even so, the y-axis correlation of spine region was larger than that of shaft region. Although FCS of EGFP5 in spines was difficult, FCS of EGFP inside dendritic spines was reproducible. The slow moving component was also detected by FCS (Fig. 9C). Next, to examine whether the slow mobile component of EGFP is appeared due to intra-spine F-actin in the same manner as EGFP5, RICS measurements were conducted before and after latrunculin A treatment (Fig. 9D-G). The variation of f_1 was analyzed with the same way as EGFP5 analysis (Fig. 8C-F). Although the magnitude of change was

smaller than EGFP5, f_1 value of spine regions increased by latrunculin A treatment (Fig. 9F, G). This result indicated that EGFP movement inside dendritic spine is also suppressed by F-actin but the suppression level for EGFP is less than that for EGFP5. The size dependence of mobility suppression is consistent with the notion that the molecular mobility inside dendritic spine is hindered by F-actin through steric interaction.

Discussion

Precise measurement of molecular mobility inside dendritic spines is important in modeling of dynamic properties of postsynaptic molecules and cytoskeletal polymers both in a resting state and after activating signaling pathways related to synaptic plasticity. In this study, I performed RICS measurements of EGFP and EGFP5 inside dendritic spines of hippocampal neurons in culture. In dendritic spines, fast and slow mobile components of both EGFP and EGFP5 were measured. The slow mobile fraction was the major component for EGFP5 and this slow mobile fraction was larger in neurons expressing EGFP5 than in neurons expressing EGFP. Depolymerization of F-actin with latrunculin A decreased the slow mobile fraction. These results demonstrated that molecular mobility is hindered by steric interaction with actin polymers inside dendritic spines.

Mobility of molecules inside dendritic spines is difficult to measure due to small size of spines. In this study, I selected RICS because RICS is a quantitative technique to detect wide range of molecular mobility inside small intracellular compartments (Digman et al., 2005, 2008). By comparing FCS and RICS, I confirmed that EGFP and EGFP5 mobility could be reliably measured using RICS at least inside larger neuronal compartments (Fig. 4). When the observation volume is in the same order of magnitude or smaller than detection volume achieved by confocal optics, the practical detection volume is reduced and the correlation function is changed (Gennerich and Schild, 2000, Foquet et al., 2004,

Sanguigno et al., 2010). The commonly-used three-dimensional diffusion models for FCS and RICS are based on the assumption that observation volume is sufficiently larger than detection volume (Rigler et al., 1993, Digman et al., 2005). Therefore, results derived from conventional physical models should be evaluated carefully and precise evaluation of diffusion within a small cytoplasmic compartment needs consideration of confinement of detection volume. In this study, I used the conventional two-component three-dimensional diffusion model for assessment of RICS correlation function because spine shape during RICS measurements and molecular process inside dendritic spines were unknown. Even with this simple model, the diffusion coefficient of fast component inside spines was comparable with that from the cytosol of soma (Fig. 4H, 5B). In addition, RICS results were not influenced by spine volume, spine neck length and cross section area (Fig. 6, 7). Therefore I concluded that semi-quantitative analysis using the conventional three-dimensional diffusion model is applicable to the analysis of dendritic spines. Of course, information of accurate spine shape and development of techniques that reduce detection volume are needed for more precise measurements (Hedde et al., 2013, Tønnensen and Nägerl, 2013).

Analyses of spines based on RICS revealed a large fraction of slowly moving EGFP5 only inside dendritic spines (Fig. 5). Previously, molecular mobility inside three dimensionally confined femtoliter volume was investigated by FCS experiments and

Monte Carlo simulation (Fowlkes and Collier, 2013). This study showed that confinement of the diffusion volume *per se* did not induce increase in a slowly moving fraction. The fraction of slow mobile component inside spines was decreased by latrunculin A treatment (Fig. 8). Latrunculin A treatment decreased the spine volume by 25% (Fig. 2D). Because the spine volume and fractional contribution of the slowly moving component were not correlated (Fig. 6), this volume reduction cannot explain the effect of latrunculin A. Dense actin filaments can suppress the mobility of molecules, of which particle radii are comparable to the mesh size of F-actin network, *in vitro* and *in vivo* (Hou et al., 1990, Wong et al., 2004, Song et al., 2009). Therefore, it is possible that F-actin-dependent suppression of molecular mobility inside spines is also dependent on the size of fluorescent probes. Consistent with this idea, suppression level for EGFP was less than that for EGFP5 inside spines (Fig. 8, 9). Because many actin binding proteins exist inside spines together with core actin polymers (Sala and Segal, 2014), it is likely that these actin interactors make the molecular meshwork denser. From these reasons, I concluded that molecular mobility is hindered by steric interaction with actin polymers inside dendritic spines. In this study, I assumed that EGFP and EGFP5 were inert probes and used them as molecular rulers. Although EGFP and tandem EGFP oligomers are usually presumed as inert probes in the cytoplasm, it is unknown whether they behave similarly within spines (Pack et al., 2006, Bancaud et al., 2009, Baum et al., 2014). If EGFP or linker within tandem oligomers

interacts with any intra-spine structures, apparent diffusion coefficient is decreased by repetitive binding and dissociation. In this situation, increase the number of EGFP or linker enhances their interaction with binding partners, resulting in size dependent decrease of apparent diffusion coefficient. To test this possibility, RICS measurements of other inert probes with their sizes comparable to or larger than EGFP5 should be performed. In addition, it should be noticed that even after latrunculin A treatment, the fractional contribution of slow moving molecules was higher in spines than in shafts (Fig. 8, 9). Spines contain various intracellular organelles, such as smooth endoplasmic reticulum and mitochondria (Hering and Sheng, 2001). These membranous structures may also suppress the molecular mobility.

F-actin organization and dynamics inside dendritic spines are critical for maintaining proper synaptic functions (Frost et al., 2010). The well-recognized function of intra-spine F-actin is regulation of spine morphology and PSD molecular composition (Allison et al., 1998, Okamoto et al., 2004, Kuriu et al., 2006, Blanpied et al., 2008, Honkura et al., 2008). In addition to these functions, I propose the molecular sieving effect of F-actin inside spines. Recently, CaMKIIα mobility inside dendritic spines was analyzed using single particle tracking photoactivated localization microscopy (Lu et al., 2014). The authors found that CaMKIIα exhibited at least three kinetic subpopulations. The diffusion coefficient of the intermediate subpopulation was between diffusion coefficient of free

diffusion molecules and that of immobile molecules, the range corresponding to the velocity of F-actin treadmilling. The size of intermediate subpopulation was profoundly decreased by latrunculin A treatment. These results indicated that intermediate mobility arose from CaMKII interaction with F-actin. CaMKII is a large holoenzyme consisting of 12 subunits (~984 kDa) (Kim et al., 2004, Lisman et al., 2012). Therefore, steric hindrance for CaMKII could be prominent inside of the actin-rich cytoplasm. My results suggest that the mobility of synaptic molecules, of which size is smaller than CaMKII holoenzyme, can be regulated by F-actin through pure steric interaction, without assuming any specific molecule-specific interactions. Molecular size of several synaptic proteins which relate to functional and structural plasticity is comparable to or larger than that of EGFP5. For example, Shank3, SynGAP, Kalirin-7 and Dreblin A are corresponded. Adding to these proteins, molecular complexes such as Arp2/3 complex are also corresponded. Since binding affinity to intra-spine structures and conformation of these proteins and protein complexes differ to EGFP5, it is worth to measure their mobility within spines and to compare with EGFP5.

Induction of long term potentiation (LTP) leads to structural changes of spines (Matsuzaki et al., 2004), which requires precise regulation of actin dynamics. During the initial phase of LTP, F-actin modifying proteins, such as Cofilin and subunits of Arp2/3 complex, accumulates inside spines (Bosch et al., 2014). These proteins reorganize F-actin

through severing and branching activities, leading to an elevation of F-actin content and spine enlargement. After this dynamic reorganization, F-actin is stabilized to sustain structural changes of spines. Along with this F-actin remodeling, spine neck becomes wider and shorter after LTP induction (Tønnesen et al., 2014). Considering the RICS results, both intra-spine F-actin remodeling and spine neck morphological change increase the rate of molecular exchange between spines and dendritic shafts. Enhanced diffusional coupling can facilitate compositional change of molecules within spines and then modulate synaptic functions. Recently, importance of SynGAP (~130 kDa) location within spine for LTP maintenance has been reported (Araki et al., 2015). SynGAP is rapidly dispersed from spines upon chemical LTP stimulation and this dispersion is a key step for the long-lasting changes in spine size. Enhanced diffusional coupling may contribute to effective SynGAP dispersion from spines. In addition to composition alternation within single spine, enhanced diffusional coupling can facilitate spreading biochemical signals to dendritic shafts and modulate synaptic crosstalk and hetero-synaptic plasticity. Activation of signaling molecules inside spines and shafts is temporally regulated along the distinct phases of synaptic plasticity (Nishiyama and Yasuda, 2015). To clarify the relationship between actin-dependent reduction of molecular mobility and the temporal regulation of signaling, RICS measurements of inert probes and signaling molecules during structural plasticity will be informative.

In summary, I showed that molecular mobility inside the dendritic spines can be measured using RICS. The mobility of proteins ranging from 30 to 150 kDa is effectively suppressed inside dendritic spines partly by steric interaction with F-actin. Thus, F-actin may act as modulator of molecular localization and signaling transduction inside spines. Further clarification of the amount, nano-scale localization, and dynamic behavior of intra-spine structures should provide insight into synaptic functions.

References

Abdisalaam S, Davis AJ, Chen DJ, Alexandrakis G (2013) Scanning fluorescence correlation spectroscopy techniques to quantify the kinetics of DNA double strand break repair proteins after γ-irradiation and bleomycin treatment. Nucleic Acids Res 42:1–14.

Allison DW, Gelfand VI, Spector I, Craig AM (1998) Role of actin in anchoring postsynaptic receptors in cultured hippocampal neurons: differential attachment of NMDA versus AMPA receptors. J Neurosci 18:2423–2436.

Araki Y, Zeng M, Zhang M, Huganir RL (2015) Rapid dispersion of SynGAP from synaptic spines triggers AMPA receptor insertion and spine enlargement during LTP. Neuron 85:173–189.

Bacia K, Haustein E, Schwille P (2014) Fluorescence correlation spectroscopy: principles and applications. Cold Spring Harb Protoc 2014:709–725.

Bancaud A, Huet S, Daigle N, Mozziconacci J, Beaudouin J, Ellenberg J (2009) Molecular crowding affects diffusion and binding of nuclear proteins in heterochromatin and reveals the fractal organization of chromatin. EMBO J 28:3785–3798.

Baum M, Erdel F, Wachsmuth M, Rippe K (2014) Retrieving the intracellular topology from multi-scale protein mobility mapping in living cells. Nat Commun 5:4494.

Blanpied TA, Kerr JM, Ehlers MD (2008) Structural plasticity with preserved topology in the postsynaptic protein network. Proc Natl Acad Sci U S A 105:12587–12592.

Bloodgood BL, Sabatini BL (2005) Neuronal activity regulates diffusion across the neck of dendritic spines. Science 310:866–869.

Bosch M, Castro J, Saneyoshi T, Matsuno H, Sur M, Hayashi Y (2014) Structural and molecular remodeling of dendritic spine substructures during long-term potentiation. Neuron 82:444–459.

Brown CM, Dalal RB, Hebert B, Digman MA., Horwitz AR, Gratton E (2008) Raster image correlation spectroscopy (RICS) for measuring fast protein dynamics and concentrations with a commercial laser scanning confocal microscope. J Microsc 229:78–91.

Chen JH, Kellner Y, Zagrebelsky M, Grunwald M, Korte M, Walla PJ (2015) Two-Photon Correlation Spectroscopy in Single Dendritic Spines Reveals Fast Actin Filament Reorganization during Activity-Dependent Growth. PLoS One 10:e0128241.

Dani A, Huang B, Bergan J, Dulac C, Zhuang X (2010) Superresolution imaging of chemical synapses in the brain. Neuron 68:843–856.

Di Rienzo C, Piazza V, Gratton E, Beltram F, Cardarelli F (2014) Probing short-range protein Brownian motion in the cytoplasm of living cells. Nat Commun 5:5891.

Digman MA, Brown CM, Sengupta P, Wiseman PW, Horwitz AR, Gratton E (2005) Measuring fast dynamics in solutions and cells with a laser scanning microscope. Biophys J 89:1317–1327.

Digman MA, Brown CM, Horwitz AR, Mantulin WW, Gratton E (2008) Paxillin dynamics measured during adhesion assembly and disassembly by correlation spectroscopy. Biophys J 94:2819–2831.

Ebihara T, Kawabata I, Usui S, Sobue K, Okabe S (2003) Synchronized formation and remodeling of postsynaptic densities: long-term visualization of hippocampal neurons expressing postsynaptic density proteins tagged with green fluorescent protein. J Neurosci 23:2170–2181.

Foquet M, Korlach J, Zipfel WR, Webb WW, Craighead HG (2004) Focal Volume Confinement by Submicrometer-Sized Fluidic Channels. Anal Chem 76:1618–1626.

Fowlkes JD, Collier CP (2013) Single-molecule mobility in confined and crowded femtolitre chambers. Lab Chip 13:877–885.

Frost NA, Kerr JM, Lu HE, Blanpied TA (2010) A network of networks: cytoskeletal control of compartmentalized function within dendritic spines. Curr Opin Neurobiol 20:578–587.

Gennerich A, Schild D (2000) Fluorescence correlation spectroscopy in small cytosolic compartments depends critically on the diffusion model used. Biophys J 79:3294–3306.

Hedde PN, Dörlich RM, Blomley R, Gradl D, Oppong E, Cato ACB, Nienhaus GU (2013) Stimulated emission depletion-based raster image correlation spectroscopy reveals biomolecular dynamics in live cells. Nat Commun 4:2093.

Hering H, Sheng M (2001) Dendritic spines: structure, dynamics and regulation. Nat Rev Neurosci 2:880–888.

Honkura N, Matsuzaki M, Noguchi J, Ellis-Davies GCR, Kasai H (2008) The Subspine Organization of Actin Fibers Regulates the Structure and Plasticity of Dendritic Spines. Neuron 57:719–729.

Hotulainen P, Hoogenraad CC (2010) Actin in dendritic spines: connecting dynamics to function. J Cell Biol 189:619–629.

Hou L, Lanni F, Luby-Phelps K (1990) Tracer diffusion in F-actin and Ficoll mixtures. Toward a model for cytoplasm. Biophys J 58:31–43.

Jiang M, Chen G (2006) High Ca^{2+}-phosphate transfection efficiency in low-density neuronal cultures. Nat Protoc 1:695–700.

Kim SA, Heinze KG, Waxham MN, Schwille P (2004) Intracellular calmodulin availability accessed with two-photon cross-correlation. Proc Natl Acad Sci U S A 101:105–110.

Kim SA, Heinze KG, Schwille P (2007) Fluorescence correlation spectroscopy in living cells. Nat Methods 4:963–973.

Kim SA, Sanabria H, Digman MA, Gratton E, Schwille P, Zipfel WR, Waxham MN (2010) Quantifying translational mobility in neurons: comparison between current optical techniques. J Neurosci 30:16409–16416.

Kinjo M, Sakata H, Mikuni S (2011) First steps for fluorescence correlation spectroscopy of living cells. Cold Spring Harb Protoc 2011:1185–1189.

Kuriu T, Inoue A, Bito H, Sobue K, Okabe S (2006) Differential control of postsynaptic density scaffolds via actin-dependent and -independent mechanisms. J Neurosci 26:7693–7706.

Lin YC, Phua SC, Lin B, Inoue T (2013) Visualizing molecular diffusion through passive permeability barriers in cells: Conventional and novel approaches. Curr Opin Chem Biol 17:663–671.

Lippincott-Schwartz J, Snapp E, Kenworthy A (2001) Studying protein dynamics in living cells. Nat Rev Mol Cell Biol 2:444–456.

Lisman J, Yasuda R, Raghavachari S (2012) Mechanisms of CaMKII action in long-term potentiation. Nat Rev Neurosci 13:169–182.

Lu HE, MacGillavry HD, Frost N a, Blanpied TA (2014) Multiple spatial and kinetic subpopulations of CaMKII in spines and dendrites as resolved by single-molecule tracking PALM. J Neurosci 34:7600–7610.

Luby-Phelps K, Taylor DL, Lanni F (1986) Probing the structure of cytoplasm. J Cell Biol 102:2015–2022.

Luby-Phelps K (2000) Cytoarchitecture and physical properties of cytoplasm: volume, viscosity, diffusion, intracellular surface area. Int Rev Cytol 192:189–221.

MacGillavry HD, Hoogenraad CC (2015) The internal architecture of dendritic spines revealed by super-resolution imaging: What did we learn so far? Exp Cell Res 335:180–186.

Matsuzaki M, Ellis-Davies GC, Nemoto T, Miyashita Y, Iino M, Kasai H (2001) Dendritic spine geometry is critical for AMPA receptor expression in hippocampal CA1 pyramidal neurons. Nat Neurosci 4:1086–1092.

Matsuzaki M, Honkura N, Ellis-Davies GCR, Kasai H (2004) Structural basis of long-term potentiation in single dendritic spines. Nature 429:761–766.

Medalia O, Weber I, Frangakis AS, Nicastro D, Gerisch G, Baumeister W (2002) Macromolecular architecture in eukaryotic cells visualized by cryoelectron tomography. Science 298:1209–1213.

Newpher TM, Ehlers MD (2009) Spine microdomains for postsynaptic signaling and plasticity. Trends Cell Biol 19:218–227.

Nishiyama J, Yasuda R (2015) Biochemical Computation for Spine Structural Plasticity. Neuron 87:63–75.

Novak IL, Kraikivski P, Slepchenko BM (2009) Diffusion in cytoplasm: effects of excluded volume due to internal membranes and cytoskeletal structures. Biophys J 97:758–767.

Okabe S, Kim HD, Miwa A, Kuriu T, Okado H (1999) Continual remodeling of postsynaptic density and its regulation by synaptic activity. Nat Neurosci 2:804–811.

Okamoto KI, Nagai T, Miyawaki A, Hayashi Y (2004) Rapid and persistent modulation of actin dynamics regulates postsynaptic reorganization underlying bidirectional plasticity. Nat Neurosci 7:1104–1112.

Pack C, Saito K, Tamura M, Kinjo M (2006) Microenvironment and effect of energy depletion in the nucleus analyzed by mobility of multiple oligomeric EGFPs. Biophys J 91:3921–3936.

Popov S, Poo MM (1992) Diffusional transport of macromolecules in developing nerve processes. J Neurosci 12:77–85.

Rácz B, Weinberg RJ (2013) Microdomains in forebrain spines: An ultrastructural perspective. Mol Neurobiol 47:77–89.

Rigler R, Mets Ü, Widengren J, Kask P (1993) Fluorescence correlation spectroscopy with high count rate and low background: analysis of translational diffusion. Eur Biophys J 22:169–175.

Rossow MJ, Sasaki JM, Digman MA, Gratton E (2010) Raster image correlation spectroscopy in live cells. Nat Protoc 5:1761–1774.

Sala C, Segal M (2014) Dendritic spines: the locus of structural and functional plasticity. Physiol Rev 94:141–188.

Sanguigno L, De Santo I, Causa F, Netti P (2010) A closed form for fluorescence correlation spectroscopy experiments in submicrometer structures. Anal Chem 82:9663–9670.

Schwille P, Haupts U, Maiti S, Webb WW (1999) Molecular dynamics in living cells observed by fluorescence correlation spectroscopy with one- and two-photon excitation. Biophys J 77:2251–2265.

Seksek O, Biwersi J, Verkman AS (1997) Translational diffusion of macromolecule-sized solutes in cytoplasm and nucleus. J Cell Biol 138:131–142.

Sharma K, Fong DK, Craig AM (2006) Postsynaptic protein mobility in dendritic spines: long-term regulation by synaptic NMDA receptor activation. Mol Cell Neurosci 31:702–712.

Sheng M, Hoogenraad CC (2007) The postsynaptic architecture of excitatory synapses: a more quantitative view. Annu Rev Biochem 76:823–847.

Song AH, Wang D, Chen G, Li Y, Luo J, Duan S, Poo MM (2009) A selective filter for cytoplasmic transport at the axon initial segment. Cell 136:1148–1160.

Star EN, Kwiatkowski DJ, Murthy VN (2002) Rapid turnover of actin in dendritic spines and its regulation by activity. Nat Neurosci 5:239–246.

Swaminathan R, Hoang CP, Verkman AS (1997) Photobleaching recovery and anisotropy decay of green fluorescent protein GFP-S65T in solution and cells: cytoplasmic viscosity probed by green fluorescent protein translational and rotational diffusion. Biophys J 72:1900–1907.

Tønnesen J, Nägerl UV (2013) Superresolution imaging for neuroscience. Exp Neurol 242:33–40.

Tønnesen J, Katona G, Rózsa B, Nägerl UV (2014) Spine neck plasticity regulates compartmentalization of synapses. Nat Neurosci 17:678–685.

Verkman AS (2002) Solute and macromolecule diffusion in cellular aqueous compartments. Trends Biochem Sci 27:27–33.

Yuste R (2010) Dendritic Spines. The MIT Press.

Wong IY, Gardel ML, Reichman DR, Weeks ER, Valentine MT, Bausch AR, Weitz DA (2004) Anomalous diffusion probes microstructure dynamics of entangled F-actin networks. Phys Rev Lett 92:178101–1.

Acknowledgements

I am deeply grateful to my supervisor, Professor Shigeo Okabe, for his thoughtful advices throughout this research. I thank Professor Katsumasa Fujita, Dr Shogo Kawano and Dr Masahito Yamanaka (Osaka University) for their technical instruction for building microscopy system, and Professor Masataka Kinjo (Hokkaido University) for the EGFP5 construct and his helpful advises for FCS experiments, Professor Yasuhiro Inoue (Kyoto University) for valuable discussion. I also thank all of the members in Department of Cellular Neurobiology for their support.

This research was supported by Grant-in-Aid for JSPS Fellows and Graduate Program for Leaders in Life Innovation (GPLLI), The University of Tokyo.

Finally, I would like to express my gratitude to my parents for their continuous encouragement and support.

Figure Legends

Figure 1. RICS correlation functions with variable diffusion coefficients

A. Calculated RICS correlation functions for D = 0.01, 0.1, 1 and 10 μm2/sec under the imaging condition using in this study. The pixel size is 17 nm. The pixel dwell time is 40 μs and line interval is 15.36 ms respectively.

B, C. Horizontal (B) and vertical (C) cross sections of RICS correlation functions (dashed lines in panel A).

Figure 2. EGFP5 was accumulated inside dendritic spines

A. Dendrites from cultured hippocampal neuron expressing EGFP5 and mRFP at 18 DIV before and 30 min after DMSO (top) or latrunculine A treatment (bottom).

B. Correlation of mRFP (R_{spine}) and EGFP5 (G_{spine}) fluorescence of spines normalized by mRFP (R_{shaft}) and EGFP5 (G_{shaft}) fluorescence of dendritic shaft respectively from neurons of panel A (42 spines for DMSO, 50 spines for latrunculin A). Values of Pearson correlation (r) were obtained by least-squares linear regression fit.

C, D. Cultured hippocampal neurons expressing mRFP and EGFP5 were imaged before and after DMSO or latrunculine-A treatment at 18 DIV (applications were started at t = 0 min; 3 cells (38, 42 and 50 spines each) for DMSO, 3 cells (40, 49 and 50 spines each) for

latrunculin A). Temporal changes of EGFP5 accumulation (C) and spine volume (D).

E. Cultured hippocampal neurons expressing EGFP or EGFP5 were stained with anti-GFP antibody and Cy3-conjugated secondary antibody at 18 DIV.

F. Comparison between ratio of EGFP-derived fluorescence signal (G) against Cy3 fluorescnce signal (R) within spines and that within shafts (50 spines and 50 shaft regions from N = 3 cells respectively).

Scale bars, 10 μm.

Figure 3. FRAP measurements within dendritic spines of EGFP or EGFP5-expressing neurons

A. Fluorescence recovery curve of EGFP after photobleaching of dendritic spines (18 DIV, 55 spines from 6 cells).

B. Fluorescence recovery curves of EGFP5 after photobleaching of dendritic spines (DMSO: 18-20 DIV, 54 spines from 6 cells, latrunculin A: 18-20 DIV, 56 spines from 6 cells).

C. Fluorescence recovery curves of EGFP5 (panel F) were fitted by two-component model.

Figure 4. Comparison between FCS and RICS measurements

A. FCS autocorrelation functions of Rhodamine 6G (Rh6G) and Dextran70kDa-

RhodamineB (Dx70-RhB) dissolved in imaging solution.

B. RICS correlation function of Dx70-RhB solution.

C-E. FCS and RICS measurements were conducted inside soma of EGFP-expressing neuron at 19 DIV. Circles indicate FCS positions and squares indicate imaging ROI for RICS (C). FCS autocorrelation functions of the red circle position in panel C (D). RICS correlation function of the red square ROI in panel C (E).

F-H. FCS and RICS measurements were conducted inside soma of EGFP5-expressing neuron at 20 DIV. Circles indicate FCS positions and squares indicate RICS ROI (F). FCS autocorrelation functions of the red circle position in panel F (G). RICS correlation function of the red square ROI in panel F (H).

Scale bars, 20 μm.

Figure 5. RICS measurements of EGFP5-expressing neurons inside dendritic spines and shafts

A. Cultured hippocampal neuron expressing EGFP5 was measured at 20 DIV. A large square indicates imaging ROI and small squares indicate RICS calculating ROI (left). RICS correlation function from the RICS ROI (center and right).

B-G. Cultured hippocampal neurons expressing EGFP5 were measured at 20 DIV (69 spines and 32 shafts regions from 5 cells). RICS correlation functions were fitted with two-

component model. Diffusion coefficients of the first (fast) component (D_1) (B), diffusion coefficients of the second (slow) component (D_2) (C) and fraction contribution of the first component (f_1) (D) from spine regions and shaft regions were compared. Correlations of D_1 with D_2 (E), D_1 with f_1 (F) and D_2 with f_1 (G). Values of Pearson correlation (r) were obtained by least- squares linear regression fit.

Scale bar, 5 μm.

Figure 6. Correlation of spine volume and RICS results

A-C. Cultured hippocampal neurons expressing EGFP5 were measured at 20 DIV (69 spines from 5cells. The data was the same as that used in Fig. 4B-G). Correlations of spine volume (spine fluorescence intensity of EGFP5) with D_1 (A), D_2 (B) and f_1 (C).

D-F. Cultured hippocampal neurons expressing EGFP5 were measured twice for 10 min interval (18-21 DIV, 23 spines from 11cells). Correlations of change of spine volume with changes of D_1 (D), D_2 (E) and f_1 (F).

Values of Pearson correlation (r) were obtained by least- squares linear regression fit.

Figure 7. Correlation of spine neck morphology and RICS results

A-F. Cultured hippocampal neurons expressing EGFP5 were measured at 20 DIV (64 spines from 5cells. The data was the same as that used in Fig. 5B-G). Correlations of spine

neck length with D_1 (A), D_2 (B) and f_1 (C). Correlations of spine neck cross section area with D_1 (D), D_2 (E) and f_1 (F).

G-I. Cultured hippocampal neurons expressing EGFP5 were measured twice for 10 min interval (18-21 DIV, 21 spines from 11cells. The data was the same as that used in Fig. 6D-F). Correlations of change of spine neck cross section with changes of D_1 (D), D_2 (E) and f_1 (F).

Values of Pearson correlation (r) were obtained by least- squares linear regression fit.

Figure 8. EGFP5 mobility inside dendritic spines was changed by latrunculin A treatment

A-B. Cultured hippocampal neuron expressing EGFP5 at 20 DIV was imaged before and 30 min after DMSO treatment (A). RICS correlation functions of the dendritic spine indicated by white arrow in panel A (B).

C-D. Cultured hippocampal neuron expressing EGFP5 at 20 DIV was imaged before and 30 min after latrunculin A treatment (C). RICS correlation functions of the dendritic spine indicated by white arrow in panel C (D).

E-F. Cultured hippocampal neurons expressing EGFP5 were imaged twice before pharmacological treatment and three times after the treatment (applications were started at t = 0 min) for 10 minutes interval (DMSO: DIV18-21, 16 spines and 11 shaft regions from

6cells, latrunculin A: DIV 19-20, 14 spines and 10 shaft regions from 5 cells). Temporal changes of the fraction contribution of the first component (f_1) of spine regions and shaft regions (E). The results from two measurements before pharmacological treatment and three measurements after pharmacological treatment were combined respectively and compared (F).

Scale bars, 5 μm.

Figure 9. EGFP mobility inside dendritic spines

A. Cultured hippocampal neuron expressing EGFP was measured at 19 DIV. Squares indicate RICS ROI.

B. RICS correlation functions from the RICS ROI in panel A.

C. FCS measurements were performed inside dendritic spines of EGFP expressing neuron at 23 DIV. FCS autocorrelation functions (center) and intensity traces (right) of the spine measurements.

D-E. Cultured hippocampal neuron expressing EGFP at 19 DIV was imaged before and 30 min after latrunculin A treatment (D). RICS correlation functions of the dendritic spine indicated by white arrow in panel D (E).

F-G. Cultured hippocampal neurons expressing EGFP were imaged twice before pharmacological treatment and three times after the treatment (applications were started at

t = 0 min) for 10 minutes interval (DMSO: DIV18-19, 12 spines and 6 shaft regions from 6cells, latrunculin A: DIV 18-20, 15 spines and 7 shaft regions from 7 cells). Temporal changes of the fraction contribution of the first component (f_1) of spine regions and shaft regions (F). The results from two measurements before pharmacological treatment and three measurements after pharmacological treatment were combined respectively and compared (G).

Scale bars, 5 μm (A, D), 2 μm (C).

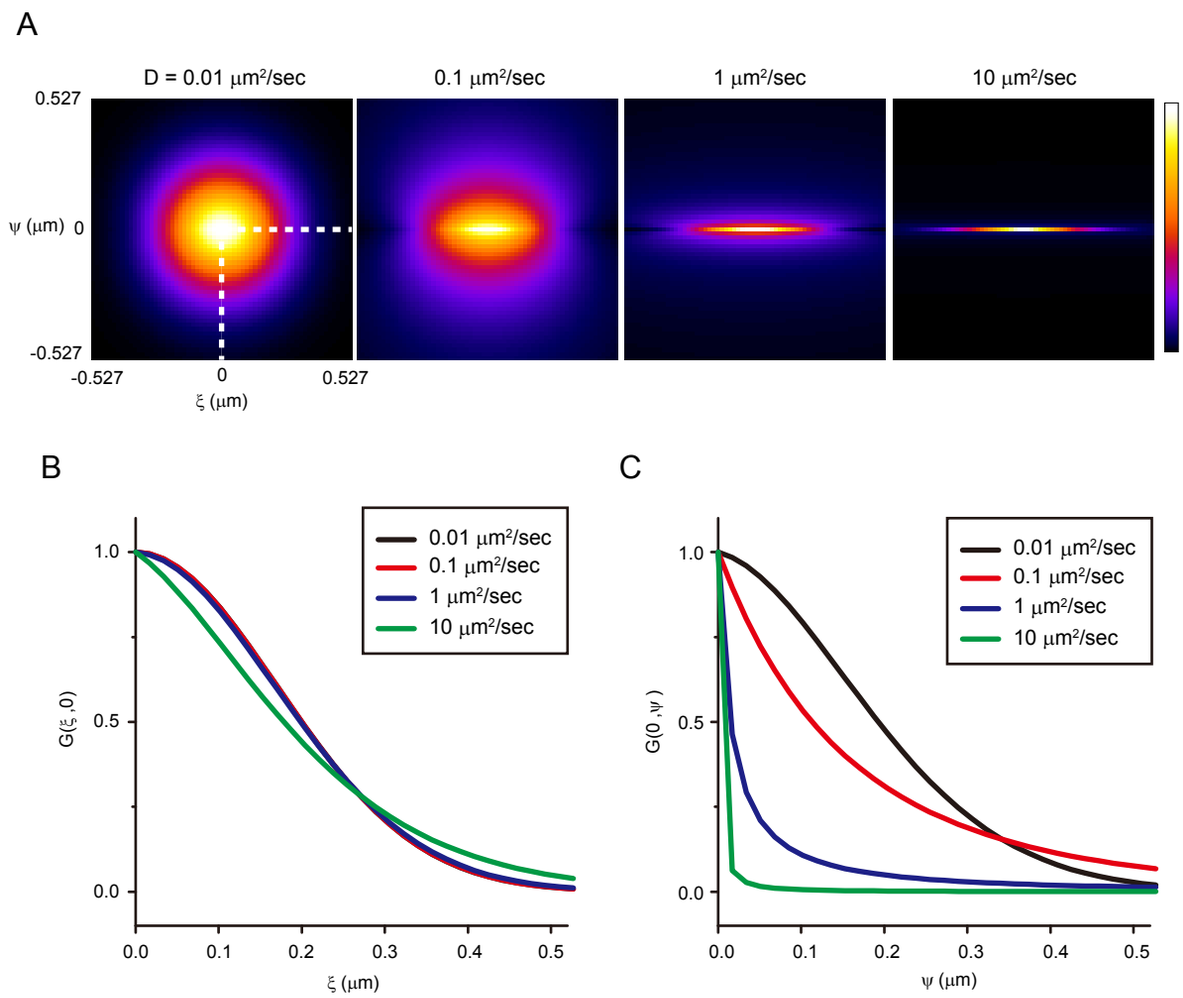
A
D = 0.01 μm²/sec
0.1 μm²/sec
1 μm²/sec
10 μm²/sec
0.527
ψ (μm) 0
-0.527
-0.527
0
0.527
ξ (μm)
B
0.01 μm²/sec
0.1 μm²/sec
1 μm²/sec
10 μm²/sec
1.0
0.5
0.0
G(ξ, 0)
0.0
0.1
0.2
0.3
0.4
0.5
ξ (μm)
C
0.01 μm²/sec
0.1 μm²/sec
1 μm²/sec
10 μm²/sec
1.0
0.5
0.0
G(0, ψ)
0.0
0.1
0.2
0.3
0.4
0.5
ψ (μm)

Figure 1

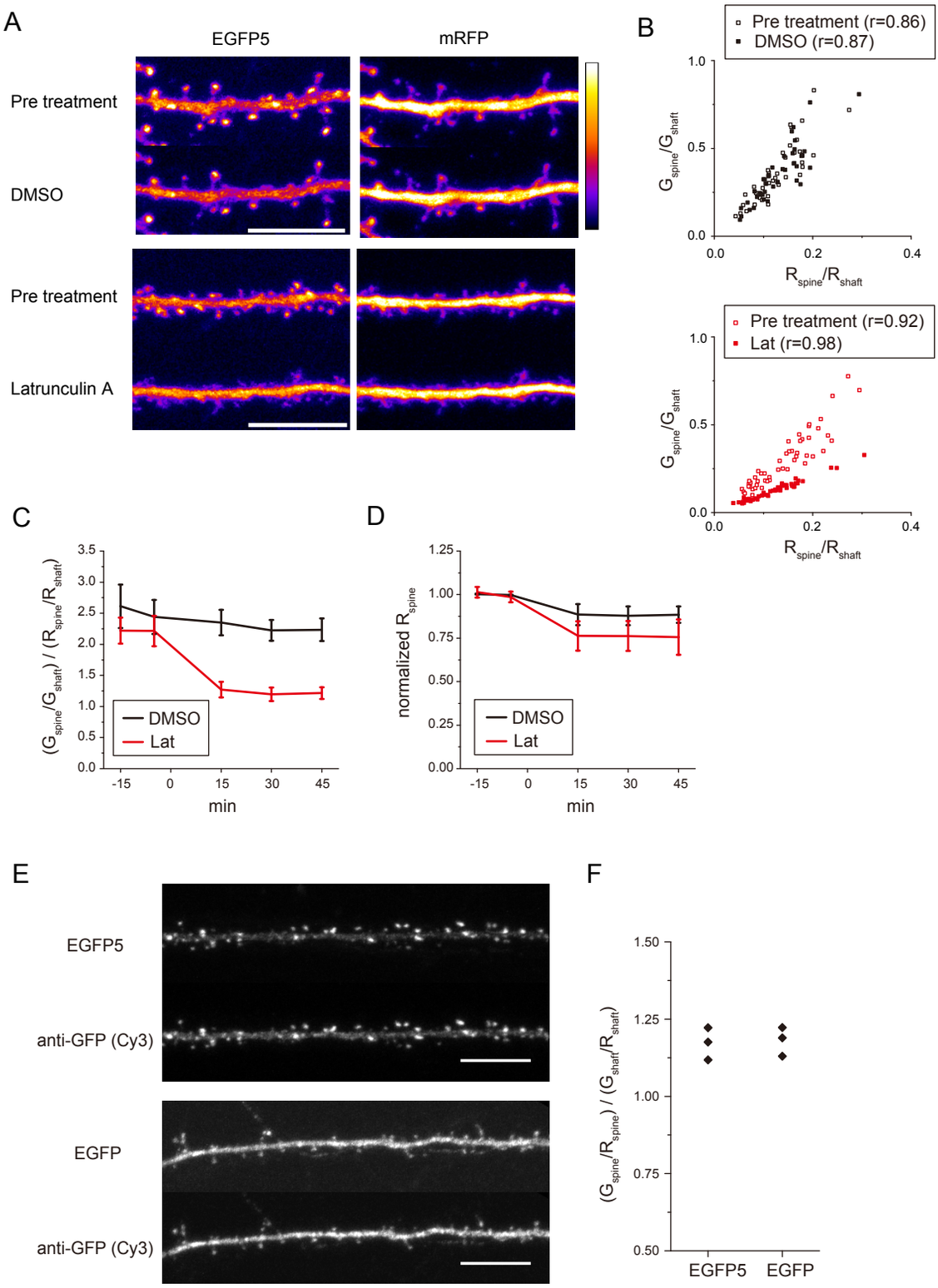
A
EGFP5
mRFP
Pre treatment
DMSO
Pre treatment
Latrunculin A
B
Pre treatment (r=0.86)
DMSO (r=0.87)
G_spine/G_shaft
R_spine/R_shaft
Pre treatment (r=0.92)
Lat (r=0.98)
C
(G_spine/G_shaft) / (R_spine/R_shaft)
DMSO
Lat
min
D
normalized R_spine
DMSO
Lat
min
E
EGFP5
anti-GFP (Cy3)
EGFP
anti-GFP (Cy3)
F
(G_spine/R_spine) / (G_shaft/R_shaft)
EGFP5
EGFP

Figure 2

A

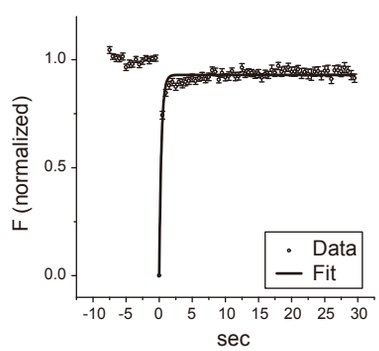

B

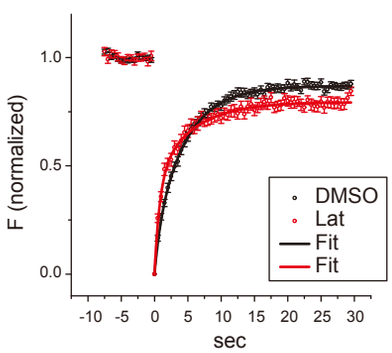

C

$F = f_1 \times \exp(-t/\tau_1) + f_2 \times \exp(-t/\tau_2) + f_3$

	f_1	f_2	f_3	τ_1 (sec)	τ_2 (sec)
DMSO	0.12 ± 0.02	0.75 ± 0.02	0.13 ± 0.01	0.43 ± 0.17	4.35 ± 0.11
Lat	0.42 ± 0.04	0.37 ± 0.03	0.21 ± 0.01	0.74 ± 0.10	5.23 ± 0.51

Figure 3

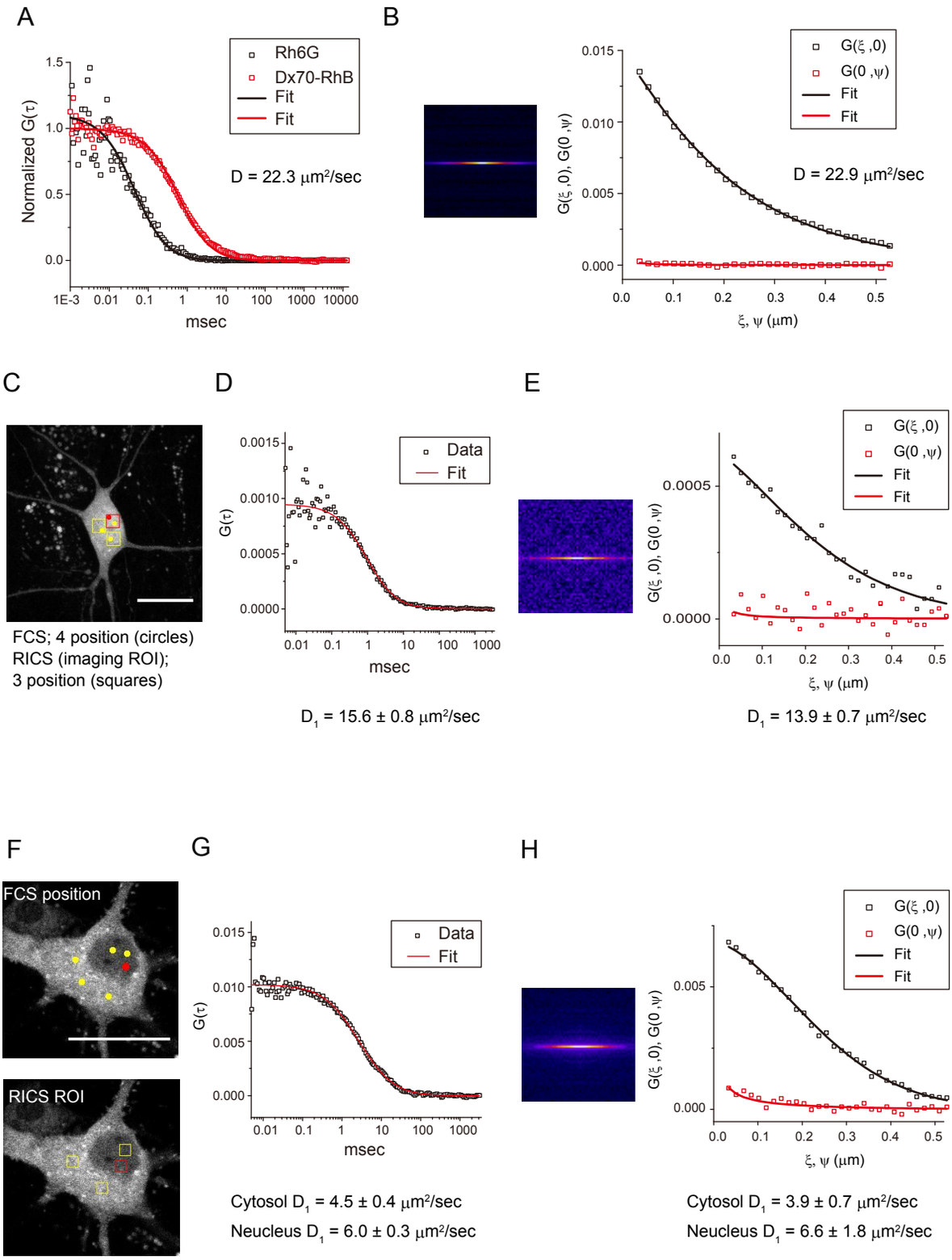
A
Rh6G
Dx70-RhB
Fit
Fit
Normalized G(τ)
msec
D = 22.3 μm²/sec
B
G(ξ ,0)
G(0 ,ψ)
Fit
Fit
G(ξ ,0), G(0 ,ψ)
ξ, ψ (μm)
D = 22.9 μm²/sec
C
FCS; 4 position (circles)
RICS (imaging ROI);
3 position (squares)
D
Data
Fit
G(τ)
msec
D1 = 15.6 ± 0.8 μm²/sec
E
G(ξ ,0)
G(0 ,ψ)
Fit
Fit
G(ξ ,0), G(0 ,ψ)
ξ, ψ (μm)
D1 = 13.9 ± 0.7 μm²/sec
F
FCS position
RICS ROI
G
Data
Fit
G(τ)
msec
Cytosol D1 = 4.5 ± 0.4 μm²/sec
Neucleus D1 = 6.0 ± 0.3 μm²/sec
H
G(ξ ,0)
G(0 ,ψ)
Fit
Fit
G(ξ ,0), G(0 ,ψ)
ξ, ψ (μm)
Cytosol D1 = 3.9 ± 0.7 μm²/sec
Neucleus D1 = 6.6 ± 1.8 μm²/sec

Figure 4

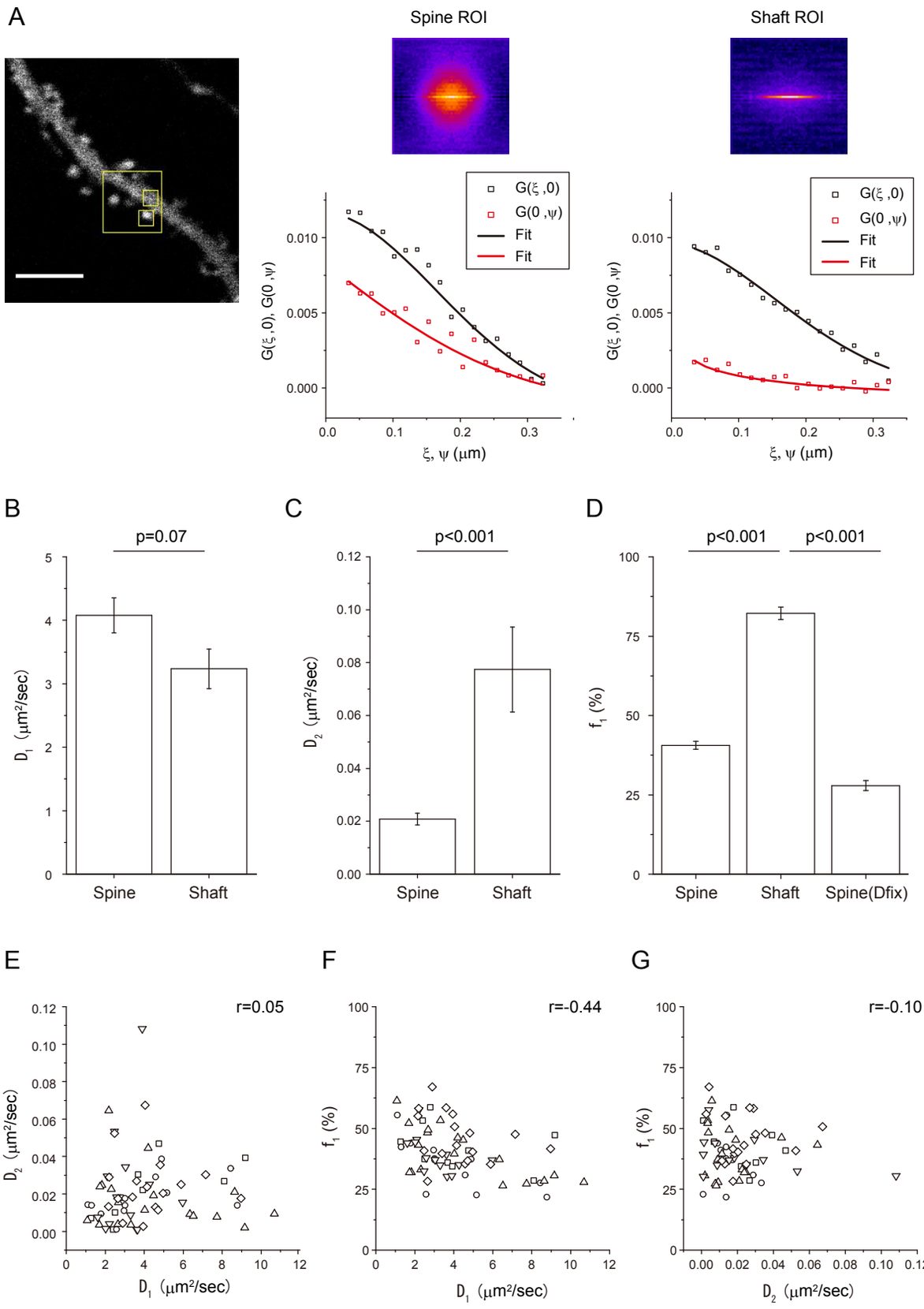
A
Spine ROI
Shaft ROI
G(ξ ,0)
G(0 ,ψ)
Fit
Fit
G(ξ ,0), G(0 ,ψ)
ξ, ψ (μm)
B
p=0.07
D1 (μm²/sec)
Spine
Shaft
C
p<0.001
D2 (μm²/sec)
Spine
Shaft
D
p<0.001
p<0.001
f1 (%)
Spine
Shaft
Spine(Dfix)
E
r=0.05
D2 (μm²/sec)
D1 (μm²/sec)
F
r=-0.44
f1 (%)
D1 (μm²/sec)
G
r=-0.10
f1 (%)
D2 (μm²/sec)

Figure 5

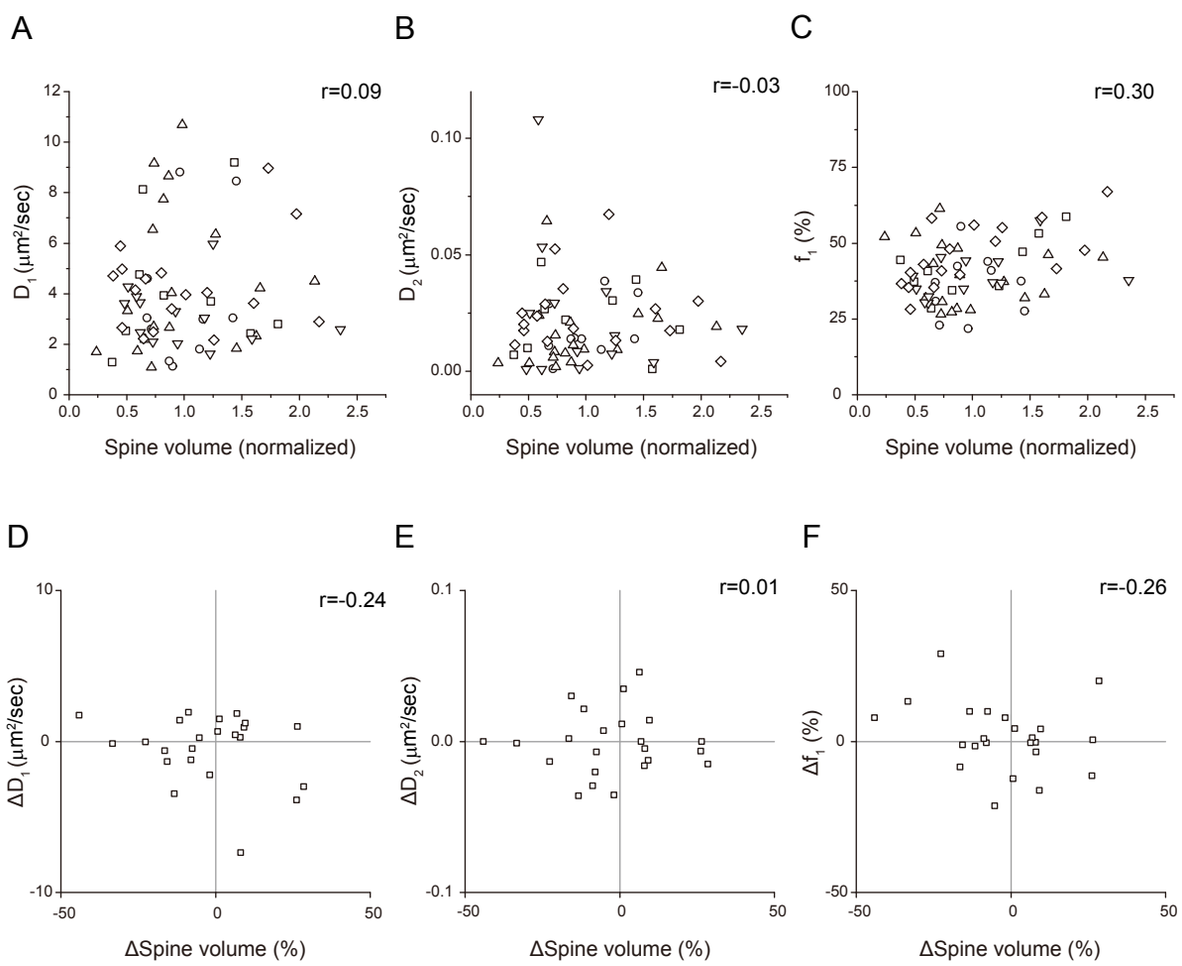
A
B
C
r=0.09
r=-0.03
r=0.30
D1 (μm²/sec)
D2 (μm²/sec)
f1 (%)
Spine volume (normalized)
Spine volume (normalized)
Spine volume (normalized)
D
E
F
r=-0.24
r=0.01
r=-0.26
ΔD1 (μm²/sec)
ΔD2 (μm²/sec)
Δf1 (%)
ΔSpine volume (%)
ΔSpine volume (%)
ΔSpine volume (%)

Figure 6

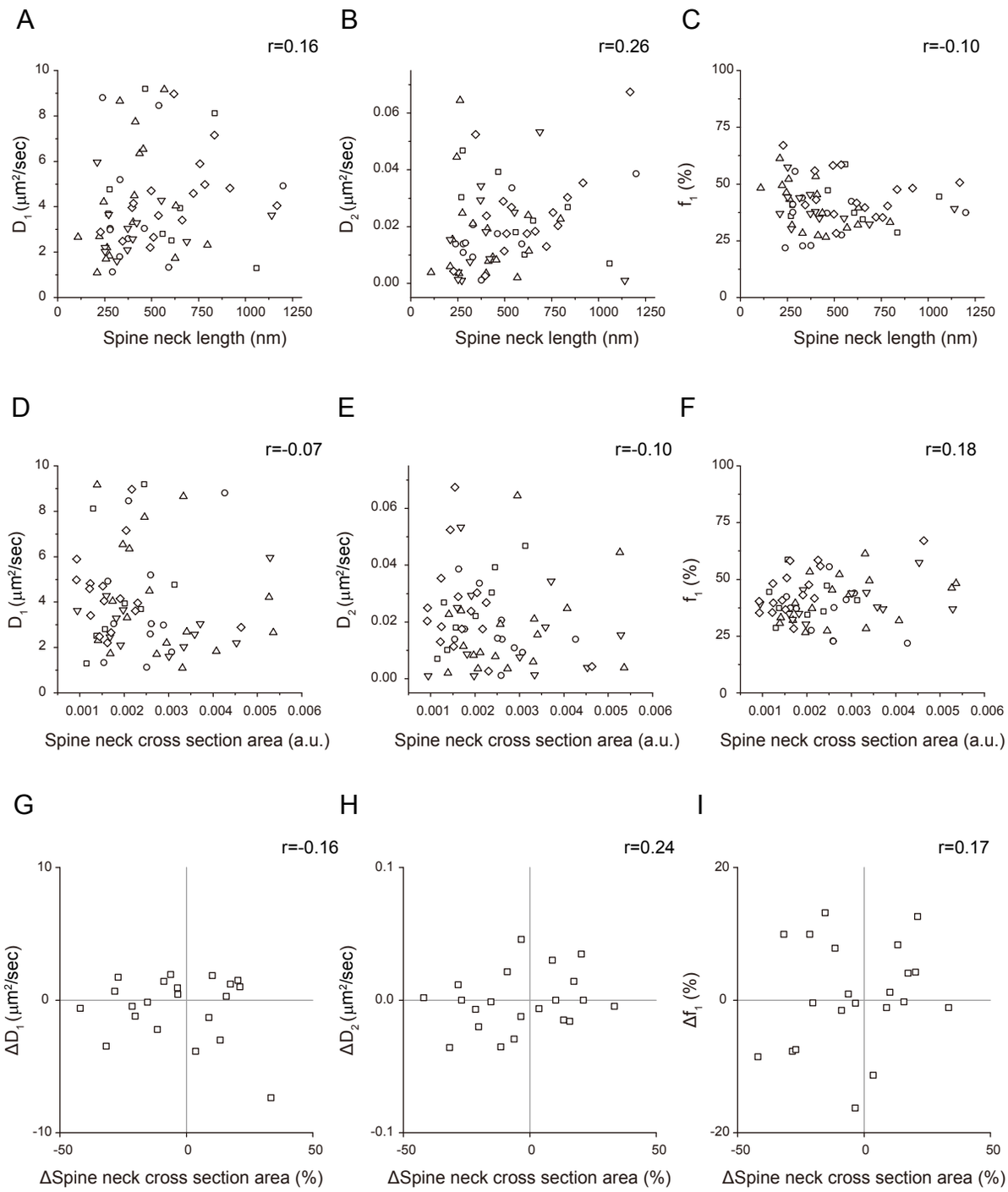
A
r=0.16
D1 (μm²/sec)
Spine neck length (nm)
B
r=0.26
D2 (μm²/sec)
Spine neck length (nm)
C
r=-0.10
f1 (%)
Spine neck length (nm)
D
r=-0.07
D1 (μm²/sec)
Spine neck cross section area (a.u.)
E
r=-0.10
D2 (μm²/sec)
Spine neck cross section area (a.u.)
F
r=0.18
f1 (%)
Spine neck cross section area (a.u.)
G
r=-0.16
ΔD1 (μm²/sec)
ΔSpine neck cross section area (%)
H
r=0.24
ΔD2 (μm²/sec)
ΔSpine neck cross section area (%)
I
r=0.17
Δf1 (%)
ΔSpine neck cross section area (%)

Figure 7

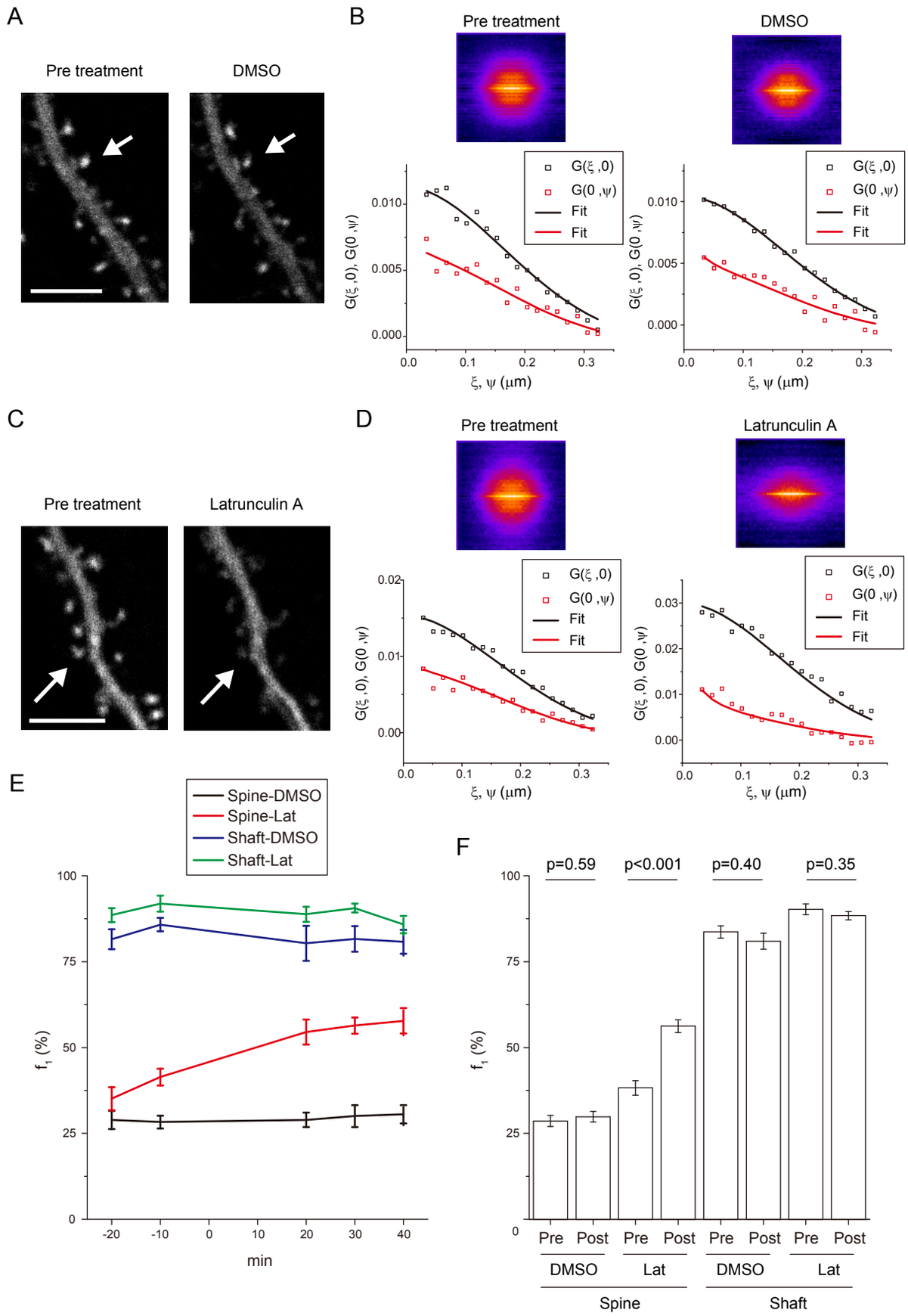
A
Pre treatment
DMSO
B
Pre treatment
DMSO
G(ξ ,0)
G(0 ,ψ)
Fit
Fit
G(ξ ,0), G(0 ,ψ)
ξ, ψ (μm)
C
Pre treatment
Latrunculin A
D
Pre treatment
Latrunculin A
E
Spine-DMSO
Spine-Lat
Shaft-DMSO
Shaft-Lat
f1 (%)
min
F
p=0.59
p<0.001
p=0.40
p=0.35
Pre
Post
DMSO
Lat
Spine
Shaft

Figure 8

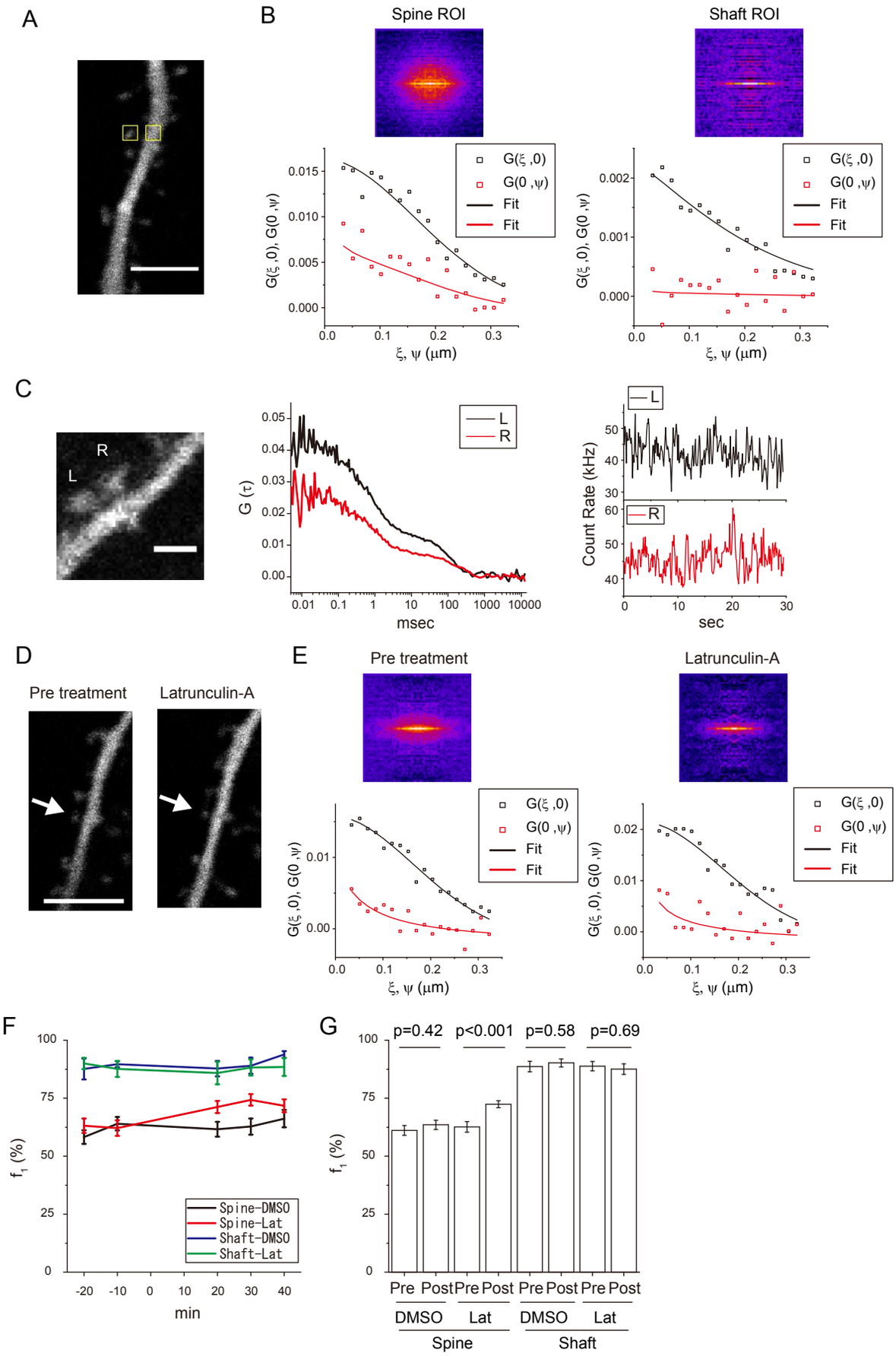
A
B
Spine ROI
Shaft ROI
G(ξ ,0)
G(0 ,ψ)
Fit
Fit
G(ξ ,0), G(0 ,ψ)
ξ, ψ (μm)
C
R
L
G (τ)
msec
Count Rate (kHz)
sec
D
Pre treatment
Latrunculin-A
E
Pre treatment
Latrunculin-A
F
f1 (%)
Spine-DMSO
Spine-Lat
Shaft-DMSO
Shaft-Lat
min
G
p=0.42
p<0.001
p=0.58
p=0.69
Pre Post Pre Post Pre Post Pre Post
DMSO Lat DMSO Lat
Spine
Shaft

Figure 9